Controlled Reduction of Bionanodots for Better Charge Storage Characteristics of Bionanodots Flash Memory

2009 Jpn. J. Appl. Phys. 48 04C190

(http://iopscience.iop.org/1347-4065/48/4S/04C190)

Controlled Reduction of Bionanodots for Better Charge Storage Characteristics of Bionanodots Flash Memory

Yosuke Tojo[1*], Atsushi Miura[1,2], Yukiharu Uraoka[1], Takashi Fuyuki[1], and Ichiro Yamashita[1,3]

[1]*Nara Institute of Science and Technology, 8916-5 Takayamacho, Ikoma, Nara 630-0192, Japan*
[2]*National Chiao Tung University, 1001 Ta-Hsueh Road, Hsinchu 30010, Taiwan*
[3]*Panasonic, 3-4 Hikaridai, Seika, Kyoto 619-0237, Japan*

Received October 1, 2008; revised December 2, 2008; accepted December 11, 2008; published online April 20, 2009

We proposed a new process technology, named the "bio-nano-process", in which semiconductor processing technology and biotechnology are conbined. We utilized a ferritin protein cobalt core as a memory node, and succeeded in performing the operation of floating gate memory. In this study, we undertook the reduction control of a cobalt core embedded in silicon oxide by thermal annealing. We also fabricated metal–oxide–semiconductor (MOS) capacitors with using the cobalt core and evaluated their electronic properties. As a result, we could elucidate the contribution of the metallic cobalt in the core by controlling of the ambient and temperature. We found that memory windows become large with increasing contribution of metallic cobalt.

DOI: 10.1143/JJAP.48.04C190

1. Introduction

Recently, attention has been focused on semiconductor-nanodot-embedded metal–oxide–semiconductor (MOS) memory devices for use in future high-speed and low-power-consumption logic and memory devices. Conventional flash memory uses a plate-type floating gate for the electric charge storage node. Utilization of the nanodot as a floating gate is a promising approach to improving device property of flash memory.[1,2] We have been demonstrating the utilization of the bionanodot (BND) as the electric charge storage node of flash memory by choosing a biochemically synthesized metal oxide nanodot formed in the vacant cavity of supramolecular cage-shaped protein ferritin.[3–7] It is well known that different kinds of inorganic nanodots, such as iron oxide, cobalt oxide, and compound semiconductor-nanodots, can be formed in the ferritin cavity by biomineralization.[8–10] We call this biomolecule-utilizing device fabrication process the bionanoprocess (BNP).[3] Here, the BNDs are synthesized as metal oxide because the synthesis process is biomineralization in aqueous solution. Therefore the reduction of embedded BNDs is necessary to achieve effective charge confinement in them in flash memory devices. For example, we have reported a functioning of embedded iron oxide BNDs (Fe-BNDs) in the MOS capacitor memory structure, that was enabled by annealing of embedded Fe-BNDs.[6] The results suggest that the conversion of oxide BND to metal BND by reduction improves the charge storage capability of flash memory with oxide BNDs. This strongly suggests the possibility of controlling the phase of the metal–oxygen complex. However, in the case of iron, changing of the reduction states is complicated.[3] In contrast, for cobalt, changing the reduction condition from cobalt oxide to metallic cobalt is simple. In this study, we examined the controlled reduction of cobalt oxide BNDs (Co-BNDs) by changing the reduction conditions, such as atmosphere and temperature. We observed the memory characteristics of Co-BND flash memory fabricated under different annealing conditions, and the reduction condition dependence of charge storage characteristics and an improvement of the charge storage capacity of Co-BND memory have been revealed.

*E-mail address: t-yosuke@ms.naist.jp

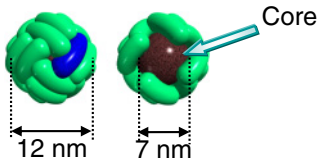

Fig. 1. (Color online) Schematic drawing of ferritin protein (left) and cross-sectional view of ferritin with BND (right).

2. Experimental Methods

Figure 1(a) depicts a schematic drawing of ferritin (left) and the cross section of Co-BND-accommodated ferritin (right). Ferritin gives several advantages for flash memory fabrication process, such as 1) uniform BND formation (approximately 7 nm) using cage-shaped ferritin protein as biotemplates; 2) high density and selective deposition owing to the self-assemble ability of protein outer surface; 3) the formation of different kinds of metal and semiconductor nanodots by replacing Fe.[9–11] The BNDs, used as charge storage nodes of memory, were synthesized in the vacant cavity of ferritin protein by biomineralization.[4,9]

Co-BND-accommodated ferritins were adsorbed on p-Si(100) substrates with 3-nm-thick thermal oxide thin film. To prevent multilayer formation, drop cast of ferritin solution was spun out in a sealed plastic tube. The outer protein shell was removed by oxidation with UV irradiation in ozone atmosphere, and a Co-BND monolayer was obtained. To prevent the re-oxidation of annealed Co-BNDs and achieve the controlled reduction of Co-BNDs, the fabricated Co-BND array was buried in thin SiO_2 film. A schematic drawing of the fabricated sample structure is shown in Fig. 2. The thickness of SiO_2 was set to 3 nm for X-ray photoelectron spectroscopy (XPS) measurements and 20 nm for the MOS capacitor. The fabricated samples were annealed inert (N_2, 100%) and reductive ($H_2 : N_2 =$ 4% : 96%) atmospheres. Samples were annealed at 350, 450, 600, 700, and 800 °C for 10 min. Annealed samples were measured by XPS and transmission electron microscopy (TEM) to confirm the reduction of embedded Co-BNDs and the morphology after high temperature annealing, respectively.

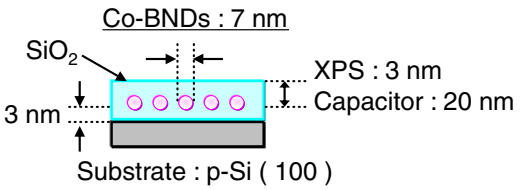

Fig. 2. (Color online) Schematic drawing of BND-embedded stacked sample structure for XPS measurement and MOS capacitor fabrication.

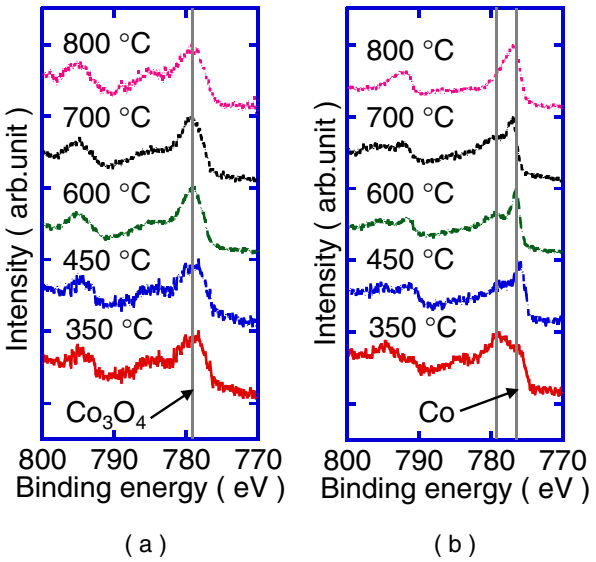

Fig. 3. (Color online) XPS spectra of annealed samples for different annealing atmospheres and temperatures. (a) N_2 (100%) and (b) H_2 (H_2 : N_2 = 4% : 96%).

We also fabricated an annealed Co-BND-embedded MOS capacitor by the same fabrication procedure as described elsewhere,[5] and high-frequency capacitance–voltage (C–V) characteristics were measured to elucidate the effect of the reduction.

3. Results and Discussion

3.1 Composition estimation

As mentioned above, the Co-BND in the protein shell was synthesized as cobalt oxide, Co_3O_4. XPS spectra of Co-BND after annealing under inert, 100% N_2 and reduction in 4% H_2 atmospheres are shown in Figs. 3(a) and 3(b), respectively. XPS spectra of Co-BNDs annealed in inert gas [Fig. 3(a)] showed a main peak at 779.5 eV. It is reported that Co_3O_4 has a Co $2p_{3/2}$ peak at 779.5 eV.[12] As we can see in XPS spectra of N_2-annealed samples, the position of the Co $2p_{3/2}$ peak shows no dependence on annealing temperature. This means that embedded Co-BNDs were not reduced even at 800 °C under inert atmosphere. In contrast to N_2 annealing, XPS spectra of H_2-annealed Co-BNDs show a new peak at 778.3 eV. This peak is assigned to $2p_{3/2}$ of metallic Co.[12] In H_2 atmosphere, the metallic Co peak appeared from 350 °C, and the increase of annealing temperature induced the decline of the Co_3O_4 peak and the increment of the metallic Co peak. Eventually, only the metallic Co peak was observed at 800 °C. These results indicated that the annealing atmosphere is more important than the annealing temperature in the control of reduction conditions of embedded BNDs. The peak intensity change after H_2 annealing suggests that the control of the reduction ratio between Co_3O_4 and metallic Co is possible by choosing appropriate annealing temperature and atmosphere. for anneal. Most of the embedded oxide-Co-BNDs were reduced to metal-Co-BNDs above 450 °C, which is the annealing temperature applied in the device fabrication process. This suggests that we can expect sufficient charge storage in the metal portion of embedded the Co-BND charge-storage node of flash memory.

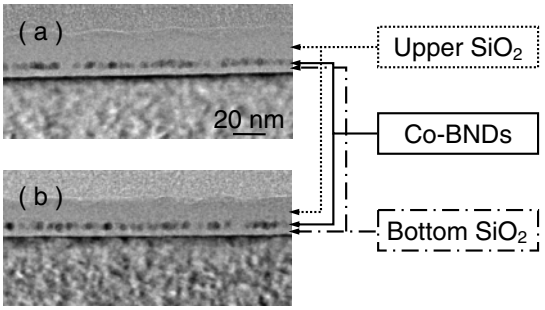

Fig. 4. (Color online) TEM images of Co-BNDs (a) before and (b) after annealing in reducing atmosphere at 800 °C.

3.2 Morphology estimation

From the viewpoint of the use of annealed BNDs in flash memory, the morphology of BNDs after high-temperature treatment should be confirmed. High-temperature treatment of a nanodot sometimes causes undesirable deformation and diffusion of the nanodot. Therefore, we performed TEM analysis, using JEM-3100FEF (JEOL), of nonannealed and annealed Co-BND in SiO_2 to check the morphology, deformation, and diffusion of Co-BND. The electron beam spot size and acceleration voltage were 0.5 nm and 300 kV, respectively. Observation positions, which are depicted in Fig. 4, of the bottom oxide, Co-BND, and the upper oxide were separated by more than 8 nm. Figure 4 depicts the cross-sectional TEM image of embedded Co-BNDs before [Fig. 4(a)] and after [Fig. 4(b)] annealing under a reducing atmosphere at 800 °C.

As seen in the TEM image of embedded Co-BNDs before annealing [Fig. 4(a)], Co-BNDs were aligned Co-BNDs with a spacing of 3–5 nm from the interface of the Si substrate and SiO_2. Co-BNDs were deposited on thermally grown SiO_2 with a thickness of ~3 nm. Therefore, the observed spacing corresponds to the thin SiO_2 layer. The observed diameter of the BNDs are almost 7 nm and they retain the spherical shape after SiO_2 deposition by plasma enhanced CVD. We have obtained a very similar TEM image for the annealed sample. Annealed Co-BNDs retain their monolayer arrangements and spherical shape even after annealing. From the analysis of the high-resolution TEM image, a slight change in the size was found after annealing.

To check the diffusion of cobalt after annealing, we performed energy dispersive X-ray spectroscopy (EDS) and elemental mapping of the same sample as depicted in Fig. 4. Figures 5(a) and 5(b) show the obtained EDS data measured before and after annealing, respectively. In the EDS data before annealing [Fig. 5(a)], we can detect the signal from

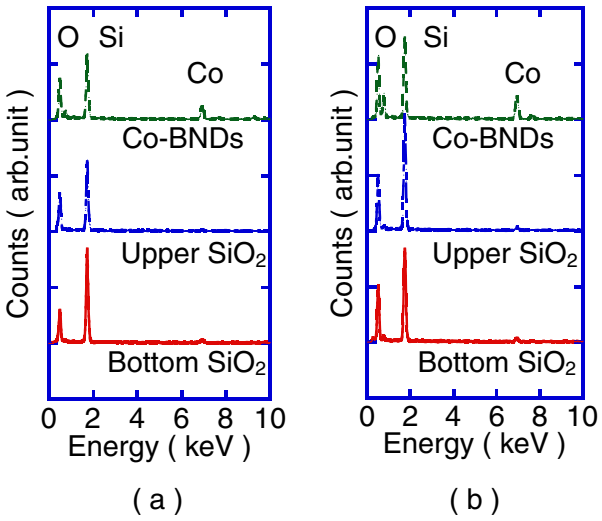

Fig. 5. (Color online) EDS spectra of embedded BND (a) before and (b) after annealing.

cobalt at 6.8 keV in the region of the Co-BND monolayer, but not in the upper and bottom oxide areas. We merely observed the signals of Si from p-Si(100) and SiO_2 and the signal of O from SiO_2 in the upper and bottom oxide areas. Cobalt is not diffused to the surrounding SiO_2 before annealing. Similar to the EDS spectra of non annealed sample, that of the annealed sample did not show any Co signal from the upper and bottom SiO_2, as shown in Fig. 5(b). This clearly indicates that Co does not diffuse to the surrounding SiO_2.

The elemental mappings shown in Fig. 6 indicate that Co does not diffuse after annealing. The mapping images of oxygen, silicon, and cobalt are depicted in Fig. 6. Figures 6(a) and 6(e) show the TEM images of the non annealed and annealed samples, respectively. Corresponding elemental mappings of O, Si, and Co before annealing are shown in Figs. 6(b) to (d), and those of after annealing are shown in Figs. 6(f) to (h), respectively. As shown in the mappings of Co in Figs. 6(d) and 6(h), no change in the distribution of Co in the stacked structure before and after annealing was observed. This indicates that Co did not diffuse even after annealing.

In general, a nano sized particle has inferior heat-resistance properties and is relatively easily decomposed by high-temperature treatment. It has been reported that BND is also decomposed by heat treatment at 700 °C.[13] In the reported case, Fe-BND and bare BND arrays were exposed to nitrogen atmosphere, i.e., without the protective film of SiO_2 applied in this study. We observed slight shrinkage of embedded Co-BNDs after high-temperature annealing. We reported a similar reduction in the size in the case of the annealing Fe-BNDs.[6] This behavior is due to the desorption of oxygen after annealing, and the shrinkage of the annealed Co-BNDs is considered to be due to a similar reason. In summary, the results of TEM measurements revealed that the Co-BNDs embedded in SiO_2 are not diffused to the surrounding SiO_2 nor collapsed, because of the protection provided by the deposited SiO_2 thin film against the applied high temperature.

3.3 Capacitance–voltage characteristics

Figure 7 shows the observed capacitance–voltage (C–V) characteristics of the fabricated Co-BND embedded MOS capacitors. The curves in Fig. 7 depict the C–V obtained for (a) the reference sample without Co-BND, (b) the sample annealed in N_2: 100% at 800 °C and (c) the sample annealed in H_2: 4% at 800 °C. The observed C–V curves are normalized with maximum capacitance to enable comparison. In the case of capacitors without Co-BND [curve (a)], no hysteresis was observed. In contrast, we observed anticlockwise hysteresis due to charge injection to the embedded Co-BND in curves (b) and (c). We observed a larger memory window in the case of the treatment under a reducing atmosphere at 800 °C [i.e., curve (c)]. It is of interest that, the Co-BND memory annealed in N_2 showed charge confinement in the embedded "cobalt oxide" BNDs, although the memory window size is not large compare with the MOS capacitors annealed in H_2. This indicates that cobalt oxide BND can also confine the charge in the MOS stacked structure. The relationship between the annealing temperature and observed memory window size (ΔV) is summarized in Fig. 8 for a memory window size extracted from the C–V characteristics of N_2- and H_2-annealed samples at different temperatures. N_2-annealed samples (depicted with circle) showed similar ΔV independent of

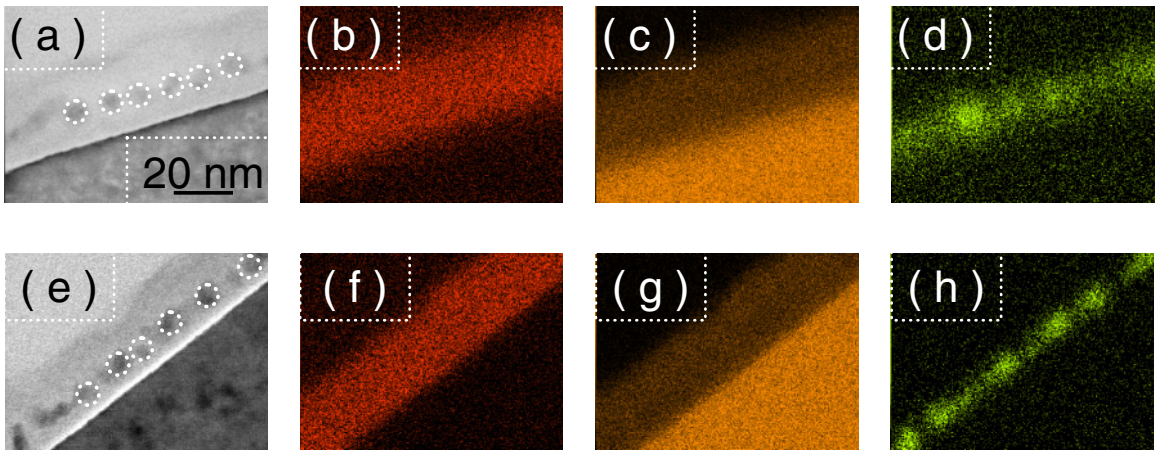

Fig. 6. (Color online) TEM images of (a) before and (e) after annealing. EDS mapping images of (b) O, (c) Si, and (d) Co before the annealing, and (f), (g), and (h) after annealing in reducing atmosphere, respectively.

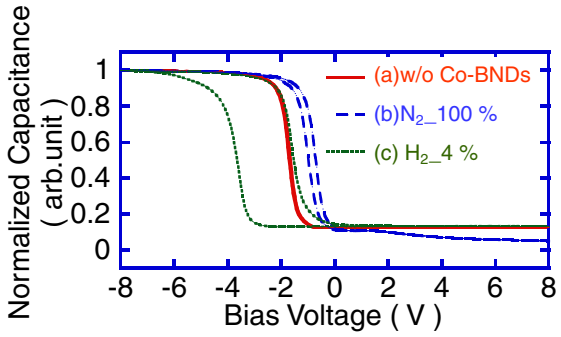

Fig. 7. (Color online) Normalized *C–V* characteristics of samples (a) without Co-BNDs, (b) after 800 °C annealing in inert atmosphere, and (c) after 800 °C annealing in reducing atmosphere.

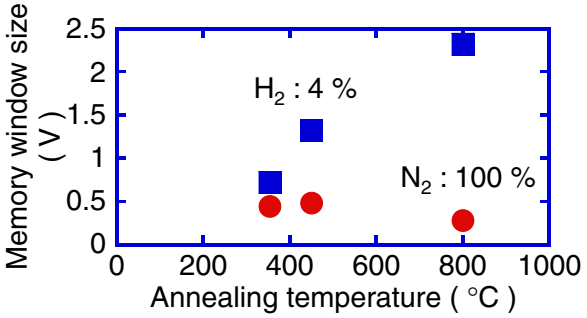

Fig. 8. (Color online) Memory window size-annealing temperature characteristics.

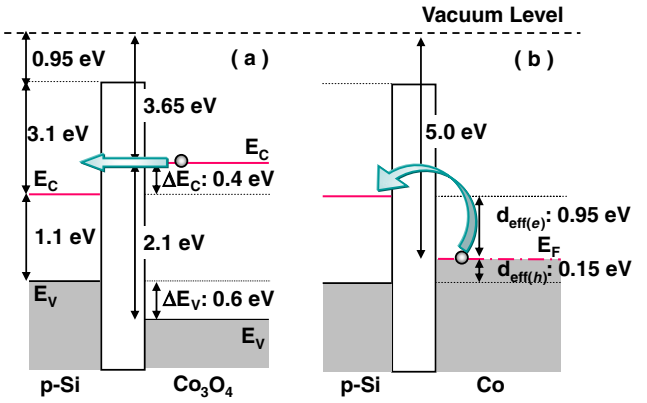

Fig. 9. (Color online) Band diagram under the flat band condition (a) Co_3O_4; (b) Co.

the annealing temperature. Instead, the ΔV of H_2 annealed MOS capacitors increased with annealing temperature. On the basis of the spectral change in XPS, the observed widening of the memory window is considered to be due to the increment of the metallic portion of Co-BND. This result suggests that the reduction of oxide Co-BND to metallic Co-BND can improve the charge storage capacity of BND flash memory.

The observed relationship between the memory window size and the annealing temperature can be explained using the band alignment diagrams under the flat band condition depicted in Fig. 9. As indicated by XPS data, Co-BNDs exist as cobalt oxide, Co_3O_4, before annealing and as metallic cobalt, Co, after annealing. Potential barriers between Si and oxide Co-BND for E_C (ΔE_C) and E_V (ΔE_V) are depicted in Fig. 9(a), respectively. The $d_{\mathrm{eff(e)}}$ and $d_{\mathrm{eff(h)}}$ are effective potential well depths of metal Co-BND for electrons and holes with respect to the E_C and E_V of Si, respectively. In the case of Co_3O_4, the conduction band energy (E_C) of Co_3O_4 is positioned at 0.4 eV higher than that of Si substrate. Therefore, the injected electrons in Co-BND will easily back-tunnel to the Si substrate when the applied gate voltage returns to the flat band condition. Therefore, the charge capacity should be poor and the memory window cannot be large. In contrast, in the case of metallic Co, the Fermi level of Co ($E_f \sim 5.0$ eV[4]) is positioned in the band gap of the Si substrate and can form the deep potential well of 0.95 eV between the E_C of Si and E_f of Co. The advantage of using a metallic nanoparticle in floating gate memory is the deeper potential well in comparison with the use of a Si nanocrystal.[14] We should note that the electron back-tunneling owing to the increase in the potential energy of charged electrons by Coulomb charging energy can be ignored in this case. The potential of metallic Co-BND increases when a single electron injection to the embedded BND is calculated on the basis of the self-capacitance of BND ($C_{\mathrm{self}} = 2\pi\varepsilon_{\mathrm{ox}}d$).[14] Here, d denotes the diameter of the dot. Coulomb charging energy gap (W) is obtained from

$$W = (ne)^2/C_{\mathrm{self}}, \quad (1)$$

where n denotes the number of electrons and e denotes the elementary charge. From the calculation of eq. (1) with $d = 7$ nm, the charging energy gap of 0.1 eV is obtained. From the analysis of the *C–V* curve, the observed memory window size 2.5–3.0 V with a dot density of 6.5×10^{11} cm^{-2}, which suggests that there are less than two stored electrons for each dot. Even after a potential increase of 0.2 eV after electron charging, the potential well depth is more than 0.7 eV. This value is sufficiently large to prevent the electron back-transfer from metallic Co-BND to the Si substrate. Therefore, better electron confinement can be achieved in BND storage node even under the flat band condition. Along with the above interpretation, the increase of the memory window size is explained as being due to the metallic Co instead of oxide Co_3O_4 in the BND stacked memory structure. The obtained results indicate that the reduction of oxide BND to metallic BND can improve the charge storage properties. The reduction of oxide BND resulted in longer charge retention in which the stored electrons were not back-transferred to the substrate under the flat band voltage condition and a larger charge storage capacity, that is obviously reflected in the memory window width of the *C–V* characteristics.

4. Conclusions

We demonstrated the controlled reduction of Co-BNDs synthesized in ferritin protein for the application to floating gate memory. We investigated the morphology, composition and memory window sizes after annealing. We confirmed that Co-BNDs were reduced to metallic Co-BND under H_2 atmosphere at relatively low temperature (~450 °C) without deforming or diffusing. We also observed that metallic Co-BND strongly contributed to the increase of the charge storage capacitance.

Acknowledgements

This work was partially supported by the Ministry of Education, Culture, Sports, Science and Technology (MEXT), "Priority Area". This work was also supported by the Leading Project by MEXT, Japan.

1) S. Tiwari, F. Rana, H. Hanafi, A. Harstein, E. F. Crabbe, and K. Chan: Appl. Phys. Lett. **68** (1996) 1377.
2) S. Tiwari, F. Rana, K. Chan, L. Shi, and H. Hanafi: Appl. Phys. Lett. **69** (1996) 1232.
3) I. Yamashita: IEDM Tech. Dig., 2006, p. 447.
4) A. Miura, Y. Uraoka, T. Fuyuki, S. Yoshii, and I. Yamashita: J. Appl. Phys. **103** (2008) 074503.
5) A. Miura, T. Hikono, T. Matsumura, H. Yano, T. Hatayama, Y. Uraoka, T. Fuyuki, S. Yoshii, and I. Yamashita: Jpn. J. Appl. Phys. **45** (2006) L1.
6) T. Hikono, T. Matsumura, A. Miura, Y. Uraoka, T. Fuyuki, M. Takeguchi, S. Yoshii, and I. Yamashita: Appl. Phys. Lett. **88** (2006) 023108.
7) K. Yamada, S. Yoshii, S. Kumagai, A. Miura, Y. Uraoka, T. Fuyuki, and I. Yamashita: Jpn. J. Appl. Phys. **46** (2007) 7549.
8) T. Dougras and M. Young: Nature **393** (1998) 152.
9) R. Tsukamoto, K. Iwahori, M. Muraoka, and I. Yamashita: Bull. Chem. Soc. Jpn. **78** (2005) 2075.
10) I. Yamashita, J. Hayashi, and M. Hara: Chem. Lett. **33** (2004) 1158.
11) K. Yoshizawa, K. Iwahori, K. Sugimoto, and I. Yamashita: Chem. Lett. **35** (2006) 1192.
12) J. F. Moulder, W. F. Stickle, P. E. Sobol, and K. D. Bomben: *Handbook of X-ray Photoelectron Spectroscopy* (Physical Electronics Division, 1979) p. 82.
13) I. Yamashita: Thin Solid Films **393** (2001) 12.
14) C. Lee, J. Meteer, V. Narayanan, and E. C. Kan: J. Electron. Mater. **34** (2005) 1.